Laser-induced polarized fluorescence in cubic yttrium sesquioxide doped with trivalent europium

J. Dexpert-Ghys and M. Faucher
Elements de Transition dans les Solides, ER060210-C.N.R.S.-1 Place A. Briand, 92190 Meudon, France
(Received 15 December 1978)

The fluorescence spectrum of Eu^{3+} in the C_2—approximately C_{2v}—site of the C-Y_2O_3 structure was recorded using a tunable dye laser to populate the $^5D_0$ level of the $4f^6$ configuration. Because the active ion occupies an anisotropic point site in an overall cubic unit cell one can make use of the Feofilov theory to interpret the experimental polarization of the emission lines. The polarized laser beam was applied perpendicular to the (111) plane of a single crystal and the polarization for each line of the $^5D_0 \rightarrow {}^7F_{1,2,3,4}$ transitions was measured. From the data the irreducible representations associated with the Stark levels can be found. In particular the transitions $A_1 \rightarrow A_1$ and $A_1 \rightarrow A_2$ can be unambiguously distinguished from $A_1 \rightarrow B_1$ and $A_1 \rightarrow B_2$. A preliminary crystal-field analysis was undertaken on the basis of the 49 ^7F_J states using an Hamiltonian (including spin-orbit coupling) written in true C_2 symmetry, that is including imaginary crystal-field parameters. To derive approximate values of the crystal-field parameters the electrostatic point-charge model was applied.

I. INTRODUCTION

Y_2O_3 crystallizes in the cubic T_h^7 space group. It is a good host material in which $4f^n$ rare-earth ions can be embedded for optical purposes, especially fluorescence under a variety of excitation conditions. The structure contains two sites for the Y^{3+} ion: a S_6 centrosymmetrical site and a C_2 site responsible for the quasitotality of the observed emission lines. No information has been obtained until now about the irreducible representations associated with the C_2 crystal-field split levels, since even though the site symmetry is low, the overall unit cell symmetry is high, forbidding any extinction whatever the observation direction.

Schaak and Koningstein[1] attempted to identify the irreducible representations associated with electronic levels of Eu^{3+} in C-Y_2O_3 utilizing the electronic Raman technique. However they succeeded only in detecting some $^5D_0 \rightarrow {}^7F_2$ lines for the S_6 site, and none associated with the C_2 site. The present work reports a new study of this material.

II. CRYSTALLOGRAPHY

The C-Ln_2O_3 structure is related to the fluorite structure MO_2. The fluorite structure can be described as an assembly of MO_8 unit cubes. The C-Ln_2O_3 structure is an assembly of two types of MO_6 unit cubes: the S_6-type cube with two missing oxygens on a body diagonal and the C_2-type cube with the oxygen vacancies on a face diagonal. There are therefore two distinct sites for the rare-earth atom, the ratio of the number of C_2 sites to the number of S_6 being 3:1. In the following we shall only attend to the most numerous C_2 site, and consider it as pseudo C_{2v}, the real symmetry being slightly distorted.

In order to carry out the theoretical study of the polarization properties of fluorescence spectra, we have to know the relation between the symmetry elements at the rare-earth site and those of the unit cell. Figure 1 is a representation of the C-Ln_2O_3 structure. The Ln atoms occupy the center of half the little unit cubes in each X, Y, or Z direction. The oxygens occupy all the vertices of these little cubes except those for which an anion vacancy is drawn. One can see that the C_2 symmetry axis of each cationic C_{2v} site is parallel to either X, Y, or Z, that is to one of the three C_4 symmetry axes of the C-Ln_2O_3 cubic unit cell. There are therefore three groups of C_{2v} sites denoted by $i=1$, 2, or 3 according to the orientation of the C_2 axis along crystallographic X, Y, or Z, respectively. Bases for the irreducible representations in each of these local C_{2v} sites are defined as z (C_2 axis), x (chosen as joining the two oxygen vacancies), and y (normal to x and z). Table I summarizes all the relations between cubic cell and point-site symmetry elements.

III. THEORETICAL POLARIZATION PROPERTIES OF THE FLUORESCENCE SPECTRUM OF Eu^{3+} in Y_2O_3

The optically active europium ion enters the Y_2O_3 lattice by substitution in yttrium sites. Its local site

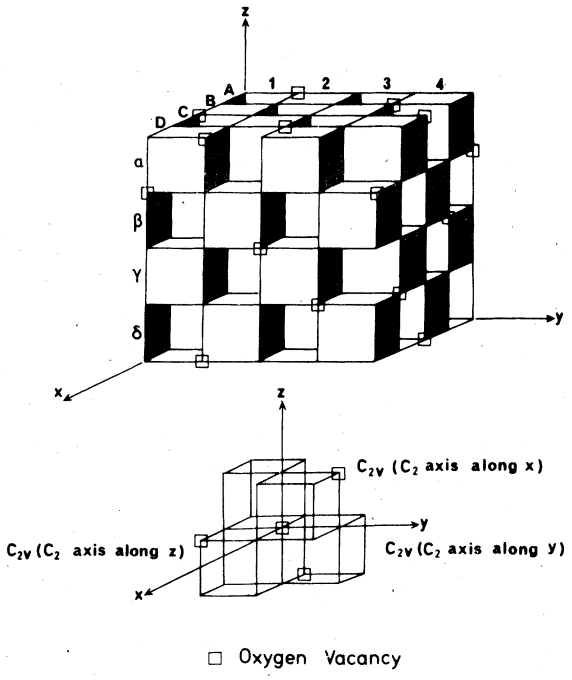

FIG. 1. C-Ln_2O_3 idealized structure (only oxygen vacancies are drawn).

symmetry is C_2, nearly C_{2v}. Subsequently to the excitation of the $^5D_0$ long-living level at 17 221 cm^{-1}, this level re-emits towards the ^7F multiplet. Table II lists the irreducible representations associated with the crystal-field splittings in C_{2v} and C_2 symmetries and the nature of the optical transitions.

The light emitted through magnetic or electric dipolar transitions is polarized either along the C_2 axis, or in the plane perpendicular to this axis. As it was said above, the C_2 symmetry axes are oriented in equal numbers along the three C_4 axes of the unit cell, so there exists no privileged direction along which some components are absent, as in uni- or biaxial crystals. However, Feofilov[2] has shown that in cubic crystals containing anisotropic centers, the degree of polarization can exceed $\frac{1}{2}$, under certain conditions of observation. The experimental evidence for this was brought in by the study of rare-earth (Eu^{3+}) doped alkali halides. Feofilov showed that the necessity for charge compensation created in fact anisotropic elementary centers. Following the azimuthal dependence of the polarization of luminescence in these crystals he established that the centers had to be oriented along the four threefold axes.

In Y_2O_3: Eu^{3+}, these centers exist without necessity of charge compensation. Feofilov's method can be applied to identify the irreducible representations associated with the Eu^{3+} levels observed in fluorescence experiments. In a first step, the absorption probabilities can be calculated by considering the clas-

TABLE I. Relations between site and unit cell symmetry elements in C-Ln_2O_3 (see Fig. 1 for notations).

Elementary cube	Site Symmetry i	Site Orientation z_i	x_i	y_i	Elementary cube	Site Symmetry i	Site Orientation z_i	x_i	y_i
$\alpha 1B$	$C_2(1)$	X	$[0\bar{1}1]$	$[011]$	$\beta 1A$	$C_2(2)$	Y	$[\bar{1}01]$	$[101]$
$\alpha 1D$	$C_2(1)$	X	$[011]$	$[0\bar{1}1]$	$\beta 1C$	$C_2(2)$	Y	$[\bar{1}01]$	$[101]$
$\alpha 2A$	S_6				$\beta 2B$	$C_2(3)$	Z	$[\bar{1}10]$	$[110]$
$\alpha 2C$	S_6				$\beta 2D$	$C_2(3)$	Z	$[110]$	$[\bar{1}10]$
$\alpha 3B$	$C_2(1)$	X	$[011]$	$[0\bar{1}1]$	$\beta 3A$	$C_2(2)$	Y	$[101]$	$[\bar{1}01]$
$\alpha 3D$	$C_2(1)$	X	$[0\bar{1}1]$	$[011]$	$\beta 3C$	$C_2(2)$	Y	$[101]$	$[\bar{1}01]$
$\alpha 4A$	S_6				$\beta 4B$	$C_2(3)$	Z	$[\bar{1}10]$	$[110]$
$\alpha 4C$	S_6				$\beta 4D$	$C_2(3)$	Z	$[110]$	$[\bar{1}10]$
$\gamma 1B$	$C_2(1)$	X	$[0\bar{1}1]$	$[011]$	$\delta 1A$	$C_2(2)$	Y	$[101]$	$[\bar{1}01]$
$\gamma 1D$	$C_2(1)$	X	$[011]$	$[0\bar{1}1]$	$\delta 1C$	$C_2(2)$	Y	$[101]$	$[\bar{1}01]$
$\gamma 2A$	S_6				$\delta 2B$	$C_2(3)$	Z	$[110]$	$[\bar{1}10]$
$\gamma 2C$	S_6				$\delta 2D$	$C_2(3)$	Z	$[\bar{1}10]$	$[110]$
$\gamma 3B$	$C_2(1)$	X	$[011]$	$[0\bar{1}1]$	$\delta 3A$	$C_2(2)$	Y	$[\bar{1}01]$	$[101]$
$\gamma 3D$	$C_2(1)$	X	$[0\bar{1}1]$	$[011]$	$\delta 3C$	$C_2(2)$	Y	$[\bar{1}01]$	$[101]$
$\gamma 4A$	S_6				$\delta 4B$	$C_2(3)$	Z	$[110]$	$[\bar{1}10]$
$\gamma 4C$	S_6				$\delta 4D$	$C_2(3)$	Z	$[\bar{1}10]$	$[110]$

sical interaction between the external electric-field $\vec{E}_0$ associated with the incident electromagnetic wave, and each elementary electric (linear oscillator) or magnetic (rotating oscillator) dipole associated with the optically active ion. In a second step, the emission probabilities of the excited oscillators in the observation direction can be calculated. The crystal orientation with respect to the incident light must be known. The results are then compared with fluorescence measurements, in which the Eu^{3+} $^5D_0$ level is excited by the linearly polarized beam of a dye laser tuned to the $^7F_0 \rightarrow {}^5D_0$ wavelength.

IV. EXPERIMENTAL

A. Materials

Y_2O_3:Eu^{3+} crystals were grown in a 2 kW solar furnace at Odeillo (France) by Dr. A. Rouanet. A mixture 99 Y_2O_3/1Eu_2O_3 (Johnson Matthey 99.99%) was melted and then gradually cooled back to room temperature in one hour. A plate-shaped crystal $2 \times 2 \times 1$ mm was chosen, the larger faces being naturally polished.

X-ray diffraction confirmed that it was a single-crystal displaying the C-Ln_2O_3 structure (cubic $a = 10.604$ Å, space group $T_h^7, Ia3$). Laue photographs gave the crystal orientation, i.e., a (111) plane parallel to the larger faces.

B. Measurements

Nonpolarized reference fluorescence spectra of Eu^{3+} were obtained under uv excitation (Osram HBO 150 W lamp equipped with a Wood filter) at 300 K, liquid nitrogen and liquid helium temperature.

Polarization measurements were performed at room temperature using a dye laser to excite selectively the $^5D_0$ level of Eu^{3+}. The basic set up is shown in Fig. 2. Excitation was accomplished by a Spectra Physics, 375/376 cw single-mode jet-stream rhodamine 6 G dye laser (1×10^{-3} M in ethyleneglycol), pumped by a Spectra Physics 164 argon ion laser. The wavelength of the laser beam is continuously tunable from about 5700 to 6500 Å. The light is vertically polarized and the linewidth is equal to 0.7 cm^{-1}.

The excitation beam was focused on the crystal, so that the (111) crystallographic plane was nearly normal to the beam direction. The light emitted by the sample was analyzed in the same direction by a Glan prism. The nearly normal incidence allows for the exciting light to be deflected from the monochroma-

TABLE II. Irreducible representations corresponding to crystalline levels in C_{2v} and C_2 site symmetry groups.

	C_{2v} (Initial Level $^5D_0$: A_1)			C_2 (Initial Level $^5D_0$: A)			
Terminating Level	Irred. Rep.	Transforms like	No. of lines	Irred. Rep.	Transforms like	No. of lines	Transition nature
$^7F_0$	A_1	z	1	A	z	1	ED
	A_2	R_z	1	A	R_z	1	
$^7F_1$	B_1	R_y	1	$2B$	R_x, R_y	2	MD
	B_2	R_x	1				
	$2A_1$	z	2	$3A$	z	3	
	A_2		/				
$^7F_2$	B_1	x	1	$2B$	x,y	2	ED
	B_2	y	1				
	A_1		/ (1)	$3A$	R_z	3	
$^7F_3$	$2A_2$	R_z	2 (/)				MD or (ED)
	$2B_1$	R_y	2 (2)	$4B$	R_x, R_y	4	
	$2B_2$	R_x	2 (2)				
	$3A_1$	z	3	$5A$	z	5	
$^7F_4$	$2A_2$		/				ED
	$2B_1$	x	2	$4B$	x,y	4	
	$2B_2$	y	2				

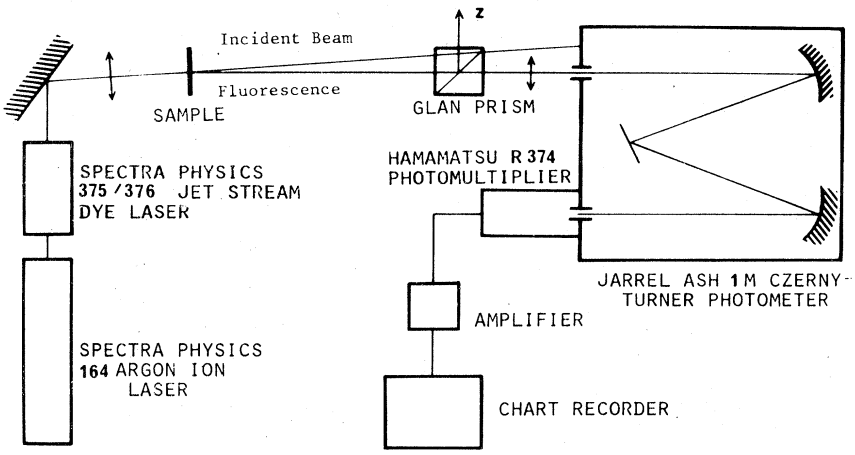

FIG. 2. Experimental apparatus.

tor entrance slit. Two fluorescence spectra were then recorded, corresponding to the $^5D_0 \rightarrow {}^7F_{1,2,3,4}$ transitions with two normal orientations of the analyzer, noted z and y.

All the fluorescence spectra were investigated with a Jarrel Ash 78460 Czerny-Turner spectrometer (focal length 1 m, reciprocal linear dispersion 4 Å/mm, in first order), and detected by an Hamamatsu R 374 photomultiplier tube.

V. CALCULATION OF THE POLARIZATION

In the following calculations we will assume an incident linearly polarized beam falling perpendicular to a (111) slab of the cubic crystal. Figure 3 represents the projection on the (111) plane of the oscillators, where α is the angle between the incident electric field $\vec{E}_0$ (as given by the dye-laser construction) and an arbitrary reference axis A connected to the crystal axis, and β is the angle between A and z (z is one direction of the analyzer). Both α and β are unspecified, but have constant values.

The total number of lines observed in the fluorescence spectrum is compatible with the C_{2v} site symmetry selection rules, so the calculations were first carried out assuming it was the true symmetry at the Eu^{3+} site. The correspondence with the C_2 group was easily made afterwards and did not change the conclusions.

A. Absorption

In our study the absorption phenomenon is always due to the $^7F_0 \rightarrow {}^5D_0$ dipolar transition. The irreducible representation corresponding to $^7F_0$ and $^5D_0$ is A_1 the electric dipolar operator is also of A_1 symmetry,

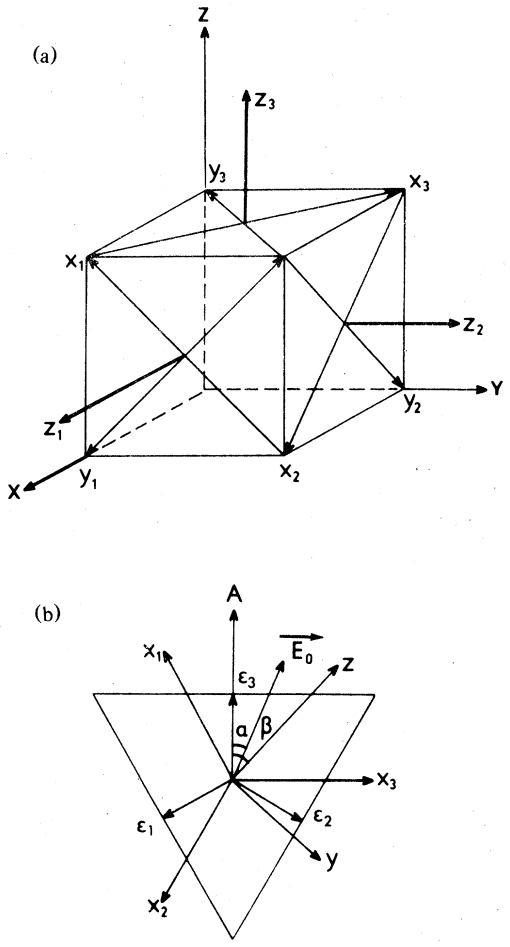

FIG. 3. (a) Possible directions for the x_i, y_i and z_i axes attached to the local oscillator and, (b) projection of the oscillators on the (111) plane.

and transforms like z_i for the ith ion. Thus the $^5D_0$ level is excited only if the external electric field $\vec{E}_0$ has a component following z_i. The probability of absorption ρ_i^a is proportional to this component and the absorption intensity to $(\rho_i^a)^2$. In practice, the three C_2 (z_i) dipoles are projected on the (111) plane (containing $\vec{E}_0$), and the interaction between the projections ($\vec{\epsilon}_i$) and $\vec{E}_0$ is calculated.

B. Emission

1. *Mechanisms of the* $^5D_0 \rightarrow {}^7F_J$ *transitions*

It is well known that $^5D_0 \rightarrow {}^7F_1$ is mainly a magnetic dipole transition (MDT), while $^5D_0 \rightarrow {}^7F_2$ is essentially an electric dipole one (EDT). For $^5D_0 \rightarrow {}^7F_3$, the character depends on the amount of admixture of $^7F_2$ and $^7F_1$ states in $^7F_3$. We only have an approximate set of crystal-field parameters (see Sec. VII) and therefore imprecise wave vectors. In practice significant contributions from both $J=1$ and $J=2$ states are present in the $^7F_3$ wave vectors. Because of this, it is impossible to ascertain whether the experimentally observed $^5D_0 \rightarrow {}^7F_3$ transition is mainly an MDT or an EDT. Only a complete intensity calculation once the true crystal-field parameters are known would be able to clarify the matter.[3] However, this ambiguity cannot change the results of polarization measurements. We shall demonstrate that $A_1 \rightarrow A_2$ lines (MDT in C_{2v} symmetry) and $A_1 \rightarrow A_1$ (EDT) behave in the same way with respect to a polarized incident beam.

A "mixed" behavior of the $^5D_0 \rightarrow {}^7F_3$ transition will only lead to a breakdown of the strict symmetry selection rules for C_{2v} (Table II) but this already arises because the true site symmetry is C_2 (see Sec. V B3), A_1 and A_2 representations become A and MDT as well as EDT are allowed.

2. *Electric dipolar transitions:* $^5D_0 \rightarrow {}^7F_2,\ {}^7F_4$

Four and seven lines are, respectively, allowed for these transitions in the C_{2v} symmetry group. Since the starting level $^5D_0$ behaves as A_1, the electric dipolar operators for $^5D_0 \rightarrow {}^7F_2$, $^7F_4$ have the same symmetry as the terminating levels, that is

$O_{ED}(A_1 \rightarrow A_1) \rightarrow A_1$, which transforms as z_i,
$O_{ED}(A_1 \rightarrow B_1) \rightarrow B_1$, which transforms as x_i,
$O_{ED}(A_1 \rightarrow B_2) \rightarrow B_2$, which transforms as y_i.

For $A_1 \rightarrow A_1$ lines, the ith ion acts as a dipole oscillating linearly along z_i. The electric-field $\vec{E}_i$ emitted in the S observation direction is oriented along a tangent to a meridian drawn on a sphere surrounding the oscillator (Fig. 4). A quantity proportional to $\vec{E}_i$ is obtained by projecting an unit vector oriented along the elementary dipole on the (111) plane. It is then decomposed into $|\vec{E}_{iy}|$ and $|\vec{E}_{iz}|$ following the two mutually perpendicular orientations of the analyzer in the experience.

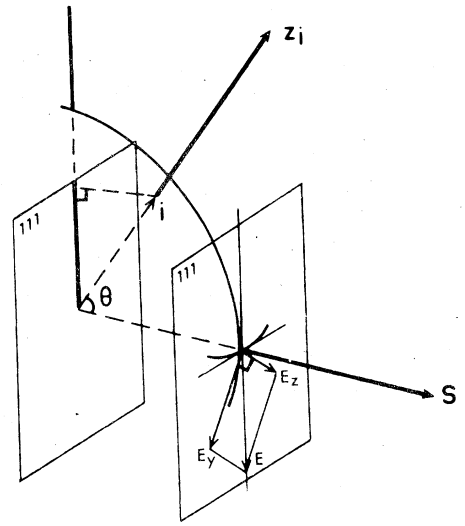

FIG. 4. Electric-field $\vec{E}_i$ emitted in the S direction by a linear dipole z_i.

The polarization is then expressed as

$$P = \frac{\sum_i (\rho_i^a)^2(|\vec{E}_{iz}|^2 - |\vec{E}_{iy}|^2)}{\sum_i (\rho_i^a)^2(|\vec{E}_{iz}|^2 + |\vec{E}_{iy}|^2)} .$$

The calculated value of P is reported in Table III.

The same calculations have to be performed for $A_1 \rightarrow B_1$ and $A_1 \rightarrow B_2$ emission lines. The Eu^{3+} ion acts as an electric dipole oscillating along x_i or y_i, respectively. Taking into account Table I one can see that in a whole cubic unit cell x_i and y_i are indistinguishable. Therefore we cannot differentiate between B_1 and B_2. For convenience we have represented in Fig. 3 x_1, x_2, and x_3 in (111) plane and y_1, y_2, and y_3 out of this plane, but in fact one has to keep in mind that for half i sites just the contrary is true.

Following the calculated values of P (Table III), we can thus identify on the one hand the $A_1 \rightarrow A_1$, and on the other hand the $A_1 \rightarrow B_1$ or B_2 fluorescence lines.

Note the individual values of α and β do not appear in the final expression of the polarization values, but only the value of $(\alpha - \beta)$, that is the angle between the incident electric field and the analyzer direction. In particular the polarization is maximum when those two directions are coincident, that is when $\alpha = \beta$.

TABLE III. Calculated values of the degree of polarization.

Absorption: Electric dipolar transition $^7F_0 \rightarrow {}^5D_0$

Irred. Rep.	Elementary Dipole	Projection on (111) Direction	Modulus	Absorption Intensity $(\rho_i^a)^2 = (\vec{\epsilon}_i \cdot \vec{E}_0)^2$
A_1	z_1	ϵ_1	$2/6^{1/2}$	$\frac{2}{3}\cos^2(2\pi/3+\alpha)$
	z_2	ϵ_2	$2/6^{1/2}$	$\frac{2}{3}\cos^2(2\pi/3-\alpha)$
	z_3	ϵ_3	$2/6^{1/2}$	$\frac{2}{3}\cos^2\alpha$

Emission: Electric dipolar transitions $^5D_0 \rightarrow {}^7F_2, {}^5D_0 \rightarrow {}^7F_4$

Irred. Rep.	Elementary Dipole	$\vec{E}i$ Emitted in the $S=[111]$ Direction: Direction	Modulus	Associated Energy $\lvert\vec{E}iz\rvert^2$	$\lvert\vec{E}iy\rvert^2$	Polarization P
A_1	z_1	ϵ_1	$2/6^{1/2}$	$\frac{2}{3}\cos^2(2\pi/3+\beta)$	$\frac{2}{3}\sin^2(2\pi/3+\beta)$	$P=\frac{1}{2}\cos2(\alpha-\beta)$
	z_2	ϵ_2	$2/6^{1/2}$	$\frac{2}{3}\cos^2(2\pi/3-\beta)$	$\frac{2}{3}\sin^2(2\pi/3-\beta)$	
	z_3	ϵ_3	$2/6^{1/2}$	$\frac{2}{3}\cos^2\beta$	$\frac{2}{3}\sin^2\beta$	
B_1	x_1	x_1	1	$\cos^2(\pi/6+\beta)$	$\sin^2(\pi/6+\beta)$	$P=-\frac{1}{4}\cos2(\alpha-\beta)$
	x_2	x_2	1	$\cos^2(\pi/6-\beta)$	$\sin^2(\pi/6-\beta)$	
	x_3	x_3	1	$\sin^2\beta$	$\cos^2\beta$	
(or B_2)	y_1	ϵ_1	$1/3^{1/2}$	$\frac{1}{3}\cos^2(2\pi/3+\beta)$	$\frac{1}{3}\sin^2(2\pi/3+\beta)$	
	y_2	ϵ_2	$1/3^{1/2}$	$\frac{1}{3}\cos^2(2\pi/3-\beta)$	$\frac{1}{3}\sin^2(2\pi/3-\beta)$	
	y_3	ϵ_3	$1/3^{1/2}$	$\frac{1}{3}\cos^2\beta$	$\frac{1}{3}\sin^2\beta$	

Emission: Magnetic dipolar transitions $^5D_0 \rightarrow {}^7F_1, {}^5D_0 \rightarrow {}^7F_3$

Irred. Rep.	Elementary Rotor	Projection of $\vec{H}_i^1$ on (111): Direction	Modulus	Associated Energy $\lvert\vec{H}_{ix}^1\rvert^2$	$\lvert\vec{H}_{iy}^1\rvert^2$	Projection of $\vec{H}_i^2$ on (111): Direction	Modulus	Associated Energy $\lvert\vec{H}_{iz}^2\rvert^2$	$\lvert\vec{H}_{iy}^2\rvert^2$	Polarization
A_2	z_1	x_1	1	$\cos^2(\pi/6+\beta)$	$\sin^2(\pi/6+\beta)$	ϵ_1	$3^{1/2}/3$	$\frac{1}{3}\cos^2(2\pi/3+\beta)$	$\frac{1}{3}\sin^2(2\pi/3+\beta)$	$P=\frac{1}{4}\cos2(\alpha-\beta)$
	z_2	x_2	1	$\cos^2(\pi/6-\beta)$	$\sin^2(\pi/6-\beta))$	ϵ_2	$3^{1/2}/3$	$\frac{1}{3}\cos^2(2\pi/3-\beta)$	$\frac{1}{3}\sin^2(2\pi/3-\beta)$	
	z_3	x_3	1	$\sin^2\beta$	$\cos^2\beta$	ϵ_3	$3^{1/2}/3$	$\frac{1}{3}\cos^2\beta$	$\frac{1}{3}\sin^2\beta$	
B_1	x_1	ϵ_1	1	$\cos^2(2\pi/3+\beta)$	$\sin^2(2\pi/3+\beta)$	...	...	...	...	$P=-\frac{1}{8}\cos2(\alpha-\beta)$
	x_2	ϵ_2	1	$\cos^2(2\pi/3-\beta)$	$\sin^2(2\pi/3-\beta)$	...	...	...	...	
(or B_2)	x_3	ϵ_3	1	$\cos^2\beta$	$\sin^2\beta$	...	...	...	...	
	y_1	x_1	1	$\cos^2(\pi/6+\beta)$	$\sin^2(\pi/6+\beta)$	ϵ_1	$2/6^{1/2}$	$\frac{2}{3}\cos^2(2\pi/3+\beta)$	$\frac{2}{3}\sin^2(2\pi/3+\beta)$	
	y_2	x_2	1	$\cos^2(\pi/6-\beta)$	$\sin^2(\pi/6-\beta)$	ϵ_2	$2/6^{1/2}$	$\frac{2}{3}\cos^2(2\pi/3-\beta)$	$\frac{2}{3}\sin^2(2\pi/3-\beta)$	
	y_3	x_3	1	$\sin^2\beta$	$\cos^2\beta$	ϵ_3	$2/6^{1/2}$	$\frac{2}{3}\cos^2\beta$	$\frac{2}{3}\sin^2\beta$	

3. *Magnetic dipolar transition:* $^5D_0 \rightarrow {}^7F_1$

For MD transitions we can say that since $^5D_0$ behaves like A_1, the magnetic dipolar operators for these transitions have the same symmetry as the terminating levels, that is,

$$O_{MD}(A_1 \rightarrow A_2) \rightarrow A_2, \text{ which transforms as } Rz_i,$$
$$O_{MD}(A_1 \rightarrow B_1) \rightarrow B_1, \text{ which transforms as } Rx_i,$$
$$O_{MD}(A_1 \rightarrow B_2) \rightarrow B_2, \text{ which transforms as } Ry_i.$$

For $A_1 \rightarrow A_2$ lines, the active ion has to be considered as an elementary magnetic rotor whose axis is along z_i. The magnetic field $\vec{H}_i$ generated in the direction S is elliptically polarized. The magnetic rotor may be resolved into two mutually perpendicular dipoles of equal amplitude oscillating in the rotor plane. These two unitary dipoles have proportional projections on the (111) plane: $\vec{H}_i^1$ and $\vec{H}_i^2$.

The analyzer measures in fact $\vec{E}_i$, so we have to make the following correspondence:

$$|\vec{E}_{iz}^n| \sim |\vec{H}_{iy}^n| \text{ and } |\vec{E}_{iy}^n| \sim |\vec{H}_{iz}^n| .$$

The polarization P following the analyzing positions y and z is then

$$P = -\frac{\sum_i (\rho_i^a)^2[(|\vec{H}_{iz}^1|^2 - |\vec{H}_{iy}^1|^2) + (|\vec{H}_{iz}^2|^2 - |\vec{H}_{iy}^2|^2)]}{\sum_i (\rho_i^a)^2[(|\vec{H}_{iz}^1|^2 + |\vec{H}_{iy}^1|^2) + (|\vec{H}_{iz}^2|^2 + |\vec{H}_{iy}^2|^2)]} .$$

The same calculations are performed for B_1 (or B_2) lines, where again, as for electric dipolar ones, there are six different directions for the elementary rotor.

The polarization values are reported in Table III. They also depend on the difference $(\alpha - \beta)$ and the polarization is maximum when the incident electric field and one direction of the analyzer are coincident. If the true symmetry group (C_2) is considered, the conclusions are not much changed. Of course, the distances and angles are slightly distorted and the values of P are not exactly those tabulated in Table III. Both B_1 and B_2 become the same irreducible representation B and the polarization sign is not changed. The only marked difference is that the $A_1 \overset{ed}{\rightarrow} A_2$ transitions become $A \rightarrow A$ and are now allowed. The corresponding electric dipolar operator behaves as an A irreducible representation, and the sign of the polarization of the corresponding lines is the same as that determined previously for A_1. In the same way $A_1 \overset{md}{\rightarrow} A_1$ also become $A \rightarrow A$; these are allowed and the sign of the polarization is the same as that of $A_1 \rightarrow A_2$.

VI. EXPERIMENTAL RESULTS

A. Fluorescence spectra

Chang and Gruber[4] obtained fluorescence spectra of Eu^{3+} ion in Y_2O_3 under uv excitation and observed several transitions originating from $^5D_0$, $^5D_1$, or $^5D_2$ electronic levels. Moreover some observed transitions could be due to the highly symmetric S_6 crystallographic site.[5,6]

Using a dye laser, selective excitation allows us to ascertain the energetic positions of $^5D_0$, $^7F_{1,2,3,4}$ levels of Eu^{3+} in the C_2 point site. Some transitions originating from the S_6 site may be observed after energy transfer. However the relative intensities of fluorescence lines selected in Table IV are the same whether we use laser or uv excitation, consequently we believe that they are to be attributed to Eu^{3+} in the same crystallographic site, namely, C_2.

By dye laser as well as uv excitation, up to five lines are observed at 77 K on the "red" shoulder of the strongest component of the $^5D_0 \rightarrow {}^7F_2$ transition (6111 Å) which is also the strongest emission line of the spectrum. Some must obviously be vibronic components. We have retained as zero-phonon lines those two that remained visible at room temperature. The one remaining line observed at 15 845 cm^{-1} makes a total of four, consistent with the C_{2v} selection rules. It also agrees with the results obtained on the isomorphous compound $Lu_2O_3:Eu^{3+}$.[7] So, the total number of observed lines (3, 4, 6, and 7, respectively, for $^5D_0 \rightarrow {}^7F_{1,2,3,4}$) is compatible with a C_{2v} point site (see Table II).

B. Polarization measurements

The intensity of the emitted light was first measured in the direction of the incident vector $\vec{E}_0$ to yield I_z, then normal to it to give I_y. Thus angles β and α are equal and, as was said above, the observed degree of polarization must be maximum. The fluorescence spectra giving Iz and Iy are recorded in Fig. 5 together with the reference spectra without the Glan prism. In Table IV are listed the peak heights (arbitrary units) which are supposedly directly proportional to the intensities. For each wavelength relative intensities are measured with exactly the same recorder sensitivity and slit aperture. Corrections must be introduced for the polarizing effect of the spectrometer, which is given by the degree of polarization of natural light passing through the spectrometer and varies with the wavelength. Using a tungsten lamp we have measured the ratio $R = I_y/I_z$ (unpolarized source) and drawn a reference curve versus wavelength. The values of P reported in Table IV are then

$$P(\text{exp}) = \frac{I_z \times R - I_y}{I_z \times R + I_y} .$$

TABLE IV. Experimental results.

Transition	uv excitation 77 K λ (Å)	uv excitation 77 K E (cm^{-1})	dye-laser excit. 77 K λ (Å)	dye-laser excit. 77 K E (cm^{-1})	dye-laser excit. 300 K λ (Å)	dye-laser excit. 300 K E (cm^{-1})	Iz	Iy	R	$P_{exp}=\frac{Iz\times R-Iy}{Iz\times R+Iy}$	Identification
$^5D_0\rightarrow{}^7F_0$	5806.0	17 224	5806.7	17 221	5807	17 221					A_1
$^5D_0\rightarrow{}^7F_1$	5874.9	17 022	5875.2	17 021	5874	17 024	108	66	1.12	+0.29	A_2
	5930.0	16 863	5931.7	16 858	5932	16 858	25	45	1.12	−0.22	
	5996.0	16 678	5998.2	16 672	5997	16 675	22	18	1.16	+0.18	
$^5D_0\rightarrow{}^7F_2$	6110.5	16 365	6110.9	16 364	6113	16 359	110	72	1.30	+0.33	A_1
	(6119)	(16 343)	(6119)	(16 343)							v
	(6122.7)	(16 332)	(6123.2)	(16 332)							v
	6128.6	16 317	6129.5	16 314	6129	16 316					
	(6137)	(16 295)	(6137)	(16 295)							v
	6144.5	16 275	6144.5	16 275	6145	16 273					
	6310.9	15 846	6311.2	15 846	6311	15 845	162	130	1.54	+0.31	A_1
$^5D_0\rightarrow{}^7F_3$	6501.5	15 381	6502.5	15 379	6505	15 373	101	104	1.82	+0.28	A_2
	6510.3	15 360	6510.0	15 360	6512	15 356					
	6527.5	15 320	6527.5	15 320	6530	15 314	19	36	1.88	−0.04	
	6576.4	15 206	6576.7	15 205	6578	15 202	12	20	1.95	+0.08	
	6622.3	15 100	6621.7	15 102	6624	15 099	38	73	2.02	+0.02	
	6637.0	15 067	6638.0	15 065	6636	15 069					A_2
$^5D_0\rightarrow{}^7F_4$	6867.5	14 561	6867.5	14 561	6872	14 552	33	37.5	2.46	+0.37	A_1
	6929.6	14 431	6930.0	14 430	6935	14 420	33	84	2.56	−0.01	
	7033.2	14 218	7034.0	14 217	7039	14 207					
	7066.4	14 151	7066.5	14 151	7070	14 144	65	90	2.81	+0.34	A_1
	7086.7	14 111	7086.5	14 111	7089	14 106	98	250	2.84	+0.05	
	7116.4	14 052	7115.5	14 054	7120	14 045	55	147	2.91	+0.04	
	7122.3	14 040	7122.5	14 040	7125	14 035	73	111	2.92	+0.31	A_1

Two $^7F_1$ lines exhibit a positive degree of polarization. However, since the magnitude of this polarization is markedly higher for the first one, the A_2 character was ascribed to the lowest energy level.

In the $^5D_0\rightarrow{}^7F_2$ transition the first strong line (16 359 cm^{-1}) is clearly of A_1-type, its polarization being strongly >0. The two next lines are much weaker and their behavior is hidden by the first one so their polarization was not established experimentally. In contrast, we can ascertain the character of two weak lines in the $^5D_0\rightarrow{}^7F_3$ transition (15 356 and 15 069 cm^{-1}) and one in the $^5D_0\rightarrow{}^7F_4$ transition (14 207 cm^{-1}), since they obviously behave in the opposite way from their strong nearest neighbors which are unambiguously assigned.

$A_1\rightarrow A_1$ lines (for an even terminal J level) or $A_1\rightarrow A_2$ (for an odd terminal J level) are theoretically strongly >0 polarized (Table III). It is noteworthy that the appropriate number of such polarized lines is observed for each transition, which permits an unambiguous identification of these components. All the $A_1\rightarrow B_1$ or $A_1\rightarrow B_2$, on the contrary, are negatively polarized with a smaller absolute value of P. This last point is less obvious in experimental results for which two subgroups should be identified (the first one with slightly >0 and the second one with slightly <0 polarization). This fact could be attributed to the real C_2 character of the site symmetry or to the imperfect quality of the single crystal. In spite of these discrepancies we think the classical theory we have applied is a valid method to assign correctly $A_1\rightarrow A_1$, A_2 transitions for Eu^{3+} in C-Y_2O_3 C_{2v} site.

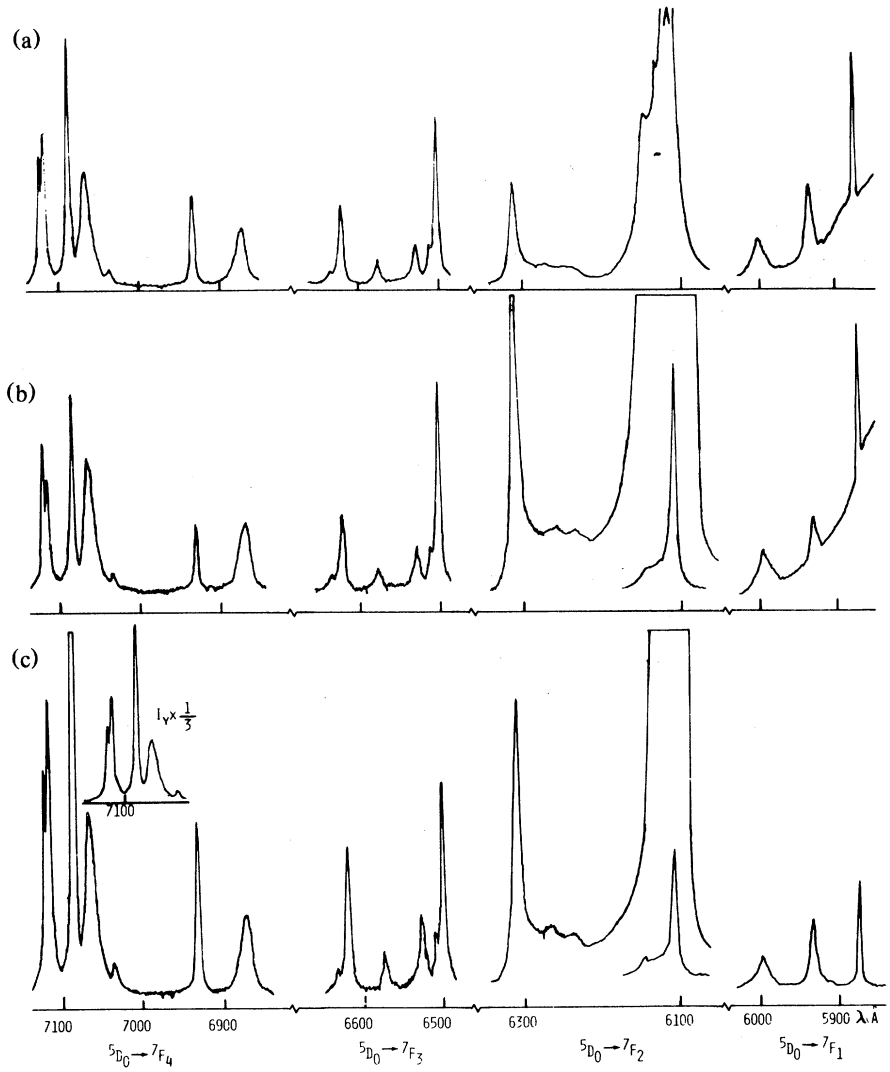

FIG. 5. Fluorescence spectra of Eu^{3+} in C-Y_2O_3 at 300 K. (a) spectrum without analyzer; (b) I_z; (c) I_y. For each line I_z and I_y are recorded under the same experimental conditions. The experimental value of the degree of polarization is given by $P = (I_z \times R - I_y)/(I_z \times R + I_y)$ (see text).

VII. PRELIMINARY CRYSTAL-FIELD ANALYSIS

The interpretation of the optical spectrum of Eu^{3+} in Lu_2O_3 has previously been carried out by Linares and Gaume-Mahn[7] and that of Er^{3+} and Tm^{3+} in Y_2O_3 by Gruber *et al.*[8] These authors studied the absorption and fluorescence spectra of single crystals of pure Tm_2O_3 and Er_2O_3 as well as 1% and 5% Er^{3+} and Tm^{3+} doped Y_2O_3. They identified 71 and 65 crystalline Stark levels for Tm^{3+} and Er^{3+}, respectively, but without polarization to give the assignment of the levels. Though J mixing was neglected, the authors succeeded in fitting the observed components and a set of calculated levels with a standard deviation equal to 13 cm^{-1}. The starting values of the B_q^k's (crystal-field parameters) for the fitting process were the PCEM (point-charge electrostatic model) calculated values.

For our crystal-field calculation, we have built up an interaction Hamiltonian acting between the 49 states of the lowest levels $^7F_{0\rightarrow 6}$ of the $4f^6$ configuration of Eu^{3+}. The ^7F manifold is well separated from the upper $^5D_0$ level (12000 cm^{-1}). This Hamiltonian includes spin-orbit coupling as well as crystal-field interaction (CFI). Spin-orbit coupling produces only diagonal terms but it locates the centers of gravity of the terms with the correct spacing to allow a good crystal-field mixing.

The matrix elements for CFI are calculated assuming the crystal-field potential can be expanded in

terms of tensor operators C_q^k to give

$$V = \sum_{kqi} B_q^k (C_q^k)_i \tag{1}$$

(Wybourne's formulation). When the site symmetry implies imaginary CFP, which is the case for C_2, Eq. (1) can be written

$$V = \sum_{k,q>0} b_q^k [C_{-q}^k + (-1)^q C_q^k] + i s_q^k [C_{-q}^k - (-1)^q C_q^k] + \sum_k b_0^k C_0^k \ , \tag{2}$$

where b_q^k and s_q^k are the real and imaginary part of B_q^k. In C_2 site symmetry, q is even and Eq. (2) reduces to

$$V = \sum_{k,q>0} b_q^k (C_{-q}^k + C_q^k) + i s_q^k (C_{-q}^k - C_q^k) + \sum_k b_0^k C_0^k \ .$$

The expression for the calculation of matrix elements following Racah's algebra may be found elsewhere.[9,10]

Let us consider two states $|J,M_J\rangle$ and $|J',M_J+q\rangle$. The only matrix elements for CFI between these two states which may be nonzero are

$$\langle J,M_J|C_{-q}^k|J',M_J+q\rangle$$

and

$$\langle J',M_J+q|C_q^k|J,M_J\rangle \ .$$

TABLE V. Crystal-field parameters determined from experimental data and PCEM calculations. (The units are cm^{-1}; b_q^k and s_q^k are the real and imaginary parts of B_q^k.)

CFP (cm^{-1})	Er^{3+} [a]	Eu^{3+} [b]	Eu^{3+} [c]
b_0^2	−154	−609 (−1220)	0
b_2^2	−608	−1213 (−470)	−4073
b_0^4	−1216	−760	−1617
b_2^4	−1496	−725	−524
s_2^4	+2	−130	0
b_4^4	+773	+616	+966
s_4^4	+18	+406	0
b_0^6	−112	+133	+352
b_2^6	+332	+29	+292
s_2^6	−25	+8	0
b_4^6	+212	+232	+658
s_4^6	−139	+111	0
b_6^6	−14	+10	−68
s_6^6	+56	+20	0

[a]CFP determined by Gruber *et al.* (Ref. 8) converted to tensor operator parameters through the relationships given by Kassman (Ref. 12).
[b]PCEM values for Eu^{3+} in Y_2O_3; s_2^2 is cancelled by a 5° rotation around Oz; between parenthesis: experimental values of b_0^2 and b_2^2.
[c]PCEM values of Eu^{3+} in an idealized Y_2O_3 structure.

Taking into account the phase factor in the expression of matrix elements and the permutation properties of the $3j$ symbols,[11] it is easy to show that in this special case ($2J$ and M_J are even), the coefficients of the imaginary parts of the B_q^k's are equal to the coefficients of the real parts in one triangle of the interaction matrix, and equal but of opposite sign in the other triangle, which of course simplifies a great deal the building up of the matrix.

Two preliminary calculations have been performed, the first one by utilizing the 14 B_q^k determined by Gruber *et al.* on Er^{3+} (Table V). The splittings of the $^7F_{1-4}$ are reported in Fig. 6 together with the experimental observed components. A second calculation was carried out, utilizing the B_q^2's deduced from the $^7F_1$ splitting in our experiments on Eu^{3+}, where

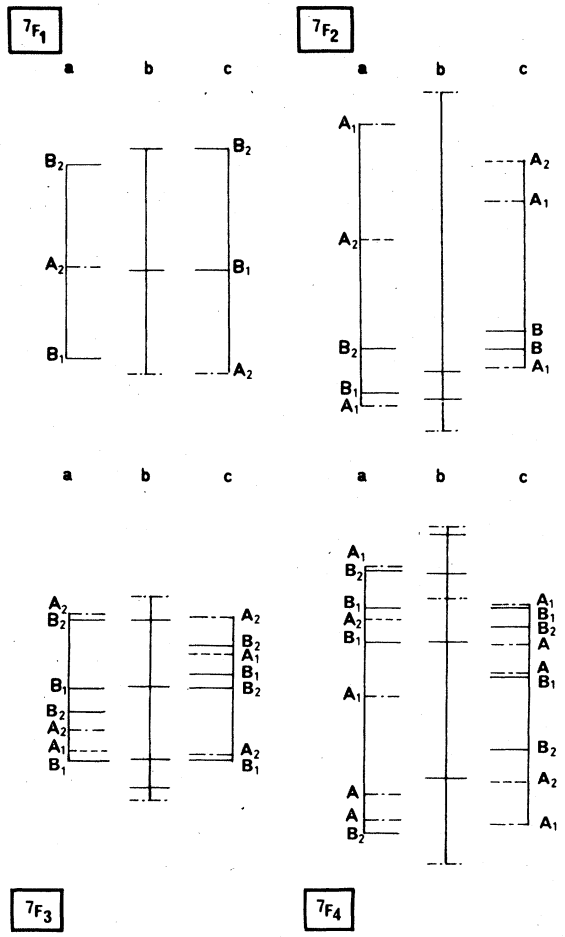

FIG. 6. Calculated and experimental energy levels of Eu^{3+} in C-Y_2O_3. (a) calculated spectrum utilizing the CFP's refined by Gruber *et al.* for Er^{3+} (Ref. 8). (b) experimental spectrum. (c) calculated spectrum utilizing experimental b_q^2's and PCEM values for the other CFP's.

the A_2 component is identified by the polarization as the lowest in energy. The other B_q^k's were given PCEM values calculated through the formula

$$B_q^k = \langle r^k \rangle e^2 \left[\frac{(k+q)!}{(k-q)!} \right]^{1/2} \sum_j \frac{g_j}{\rho_j^{k+1}} \frac{(1-x_j^2)^{-q/2}}{2^k k!} \frac{\partial^{k-q}}{\partial x_j^{k-q}} (x_j^2-1)^k e^{-iq\beta_j} \ .$$

The point charges (coordinates: ρ_j, α_j, β_j, and $x_j = \cos\alpha\hat{j}$) are arranged around the Eu^{3+} ion substituted to Y^{3+} according to the structural data of Y_2O_3 (Ref. 13) space group T_h^7:

Ln^{3+} in $8b$ (S_6 site) ,

Ln^{3+} in $24d$ (C_2 site) $x = 0.97$,

O^{2-} in $48c$ $x = 0.385$, $y = 0.145$, $z = 0.38$.

Freeman and Watson's values of the $\langle r^k \rangle$'s (Ref. 14) were introduced in the formula.

The B_q^k's given by the PCEM calculation after convergence within a sphere 30 Å in radius are reported in Table V (see b). Also given are the results of the calculation if the Y_2O_3 structure is idealized, i.e., with the following atomic positions:

Ln^{3+} in $24d$ $x = 1$,

O^{2-} in $48c$ $x = 0.375$, $y = 0.125$, $z = 0.375$.

The first shell of neighbors is exactly cubic with two oxygens missing on a face diagonal. The site symmetry is truly C_{2v} and imaginary CFP are of course missing. B_0^2 vanishes while the B_0^4/B_4^4 and B_0^6/B_4^6 ratios assume the cubic values $-(\frac{14}{5})^{1/2}$ and $+(\frac{2}{7})^{1/2}$. The reason for this can easily be found by applying the superpositon principle.

The energy levels calculated with the B_q^k's from Table V (see b) are also drawn in Fig. 6 beside the experimentally observed components. Although the true C_2 symmetry was considered, the levels retain more or less their C_{2v} character, which is why we have distinguished B_1 from B_2 and A_1 from A_2 whenever possible, but one must keep in mind it is only an approximation.

As usual the B_q^4 and B_q^6 CFP calculated by the point-charge model are too small to give a good account of the ^7F_J splittings. However, it is noteworthy that the A level positions according to our calculation are consistent with the polarization data except for an interchange between A and B levels at the bottom of $^7F_3$. It is obvious that PCEM values are only a crude starting point and the CFP need to be carefully refined which will be done shortly.

ACKNOWLEDGMENTS

The authors wish to thank Dr. J. Duran (Ecole Supérieure de Physique et Chimie de Paris, Laboratoire d'Optique) for suggesting the method. They are greatly indebted to Dr. A.Rouanet (Laboratoire des Ultra-Réfractaires, CNRS, Odeillo, France) for growing the crystal used in this investigation and to Mr. A. Malmanche (Laboratoire de Magnétisme, CNRS, Meudon, France) who determined the orientation of the sample by x-ray measurements. They wish to thank Mrs. C. Allileche and Mr. M. Fromaget for technical assistance in the preparation of the manuscript.

[1]G. Schaack and J. A. Koningstein, J. Opt. Soc. Am. 60, 1110 (1970).
[2]P. P. Feofilov, *The Physical Basis of Polarized Emission* (Consultants Bureau, New York, 1961).
[3]P. Porcher and P. Caro, J. Chem. Phys. 68, 4176 (1978).
[4]N. C. Chang and J. B. Gruber, J. Chem. Phys. 41, 3227 (1964).
[5]H. Forest and G. Ban, J. Electrochem. Soc. 116, 474 (1969).
[6]H. Forest and G. Ban, J. Electrochem. Soc. 118, 1999 (1971).
[7]C. Linares and F. Gaume-Mahn, C. R. Acad. Sci. Ser. B 265, 70 (1967).
[8]J. B. Gruber, W. F. Krupke, and J. M. Poindexter, J. Chem. Phys. 41, 3363 (1964).
[9]B. G. Wybourne, *Spectroscopic Properties of Ions in Crystals* (Interscience, New York, 1965).
[10]P. Caro, *Structure Electronique des Eléments de Transition* (Presses Universitaires de France, Paris, 1976).
[11]M. Rotenberg, R. Bivins, N. Metropolis, and J. K. Wooten, Jr., *The 3j and 6j Symbols* (MIT, Cambridge, Mass., 1959).
[12]A. J. Kassman, J. Chem. Phys. 53, 4118 (1970).
[13]F. S. Galasso, *Structure and Properties of Inorganic Solids* (Pergamon, New York , 1970), p. 101.
[14]A. J. Freeman and R. E. Watson, Phys. Rev. 127, 2058 (1962).